


Cite this: *RSC Adv.*, 2021, 11, 18074

Received 13th April 2021  
Accepted 10th May 2021

DOI: 10.1039/d1ra02884g

rsc.li/rsc-advances

# Synthesis of Co<sub>2</sub>FeGe Heusler alloy nanoparticles and catalysis for selective hydrogenation of propyne†

Takayuki Kojima,<sup>‡</sup> Yuki Nakaya,<sup>c</sup> Hyungwon Ham,<sup>c</sup> Satoshi Kameoka<sup>b</sup> and Shinya Furukawa<sup>‡\*c</sup>

Although intermetallic compounds are attracting attention of catalysis researchers, ternary intermetallic catalysts have scarcely been investigated due the difficulty of synthesizing supported nanoparticles. In this study, we successfully synthesized SiO<sub>2</sub> supported Co<sub>2</sub>FeGe Heusler alloy nanoparticles. This catalyst exhibited high catalytic performance for selective hydrogenation of propyne by nano-sizing.

An alloy is a solid mixture of two or more metallic elements. It is typically categorized into a solid solution and an intermetallic compound. In the former, different metal atoms randomly occupy lattice points, and the available range of chemical compositions is wide. In the latter, different metal atoms occupy specific lattice points, forming an ordered structure, and chemical compositions available are restricted to integer ratios. Thus, intermetallic compounds have unique electronic structures and unique atomic ordered surfaces, which are completely different from those of pure metals and solid solutions, resulting in novel catalytic properties.<sup>1–6</sup>

Along with a recent increasing interest in intermetallic catalysts, many binary compounds have been investigated as catalysts thus far; however, ternary compounds have scarcely been reported as catalysts. The number of possible elemental sets forming intermetallic compounds is much larger in ternary systems than binary ones.<sup>7</sup> In addition, novel properties originating from synergy among different elements are more likely in ternary than binary systems; for example, in the La(Co or Ru) Si catalyst for ammonia synthesis, the hydrogen storage ability, the electride property, and the electron transfer from La to the active element (Co or Ru) are believed to play key roles.<sup>8,9</sup> Therefore, the discovery of various new catalysts is expected in ternary systems.

Heusler alloys are a group of ternary intermetallic compounds described by X<sub>2</sub>YZ with L<sub>21</sub> structure (body-centered cubic basis) typically consisting of 8–12, 3–8, and 13–15 group elements for X, Y, and Z, respectively. This intermetallic group is popular as magnetic, thermoelectric, shape memory and topological materials while we have opened its new function as catalysts.<sup>10–14</sup> For selective hydrogenation of alkynes, Co<sub>2</sub>FeGe Heusler alloy showed intrinsically high alkene selectivity; that is, it selectively hydrogenated alkynes but hardly hydrogenated alkenes even for hydrogenation of alkene reactants without alkynes.<sup>11</sup> In addition, the systematic control of catalytic properties by elemental substitution (Co<sub>2</sub>Mn<sub>x</sub>Fe<sub>1–x</sub>–Ga<sub>y</sub>Ge<sub>1–y</sub>) was demonstrated. However, these catalysts were unsupported micron-sized powders with low surface areas (<0.1 m<sup>2</sup> g<sup>–1</sup>) synthesized by metallurgical process (arc melting, annealing, crushing), which were far from being of practical use. Thus, synthesis of Co<sub>2</sub>FeGe nanoparticles on solid supports, the standard form of catalysts assuring high activity per material cost, is desired.

To synthesize supported intermetallic nanoparticles, much effort is required to optimize the synthesis conditions, especially in ternary systems. For Heusler alloys, supported nanoparticles with sufficient quality (small average size with sharp distribution of sizes, small second phases, ordering into L<sub>21</sub> structure) have been reported only for Co<sub>2</sub>FeGa<sup>15–18</sup> and Cu<sub>2</sub>NiSn,<sup>19</sup> the former of which was not for catalysts but mainly for magnetic materials. Thus, synthesizing supported Co<sub>2</sub>FeGe nanoparticles with excellent catalytic properties for selective hydrogenation of alkynes is challenging. Nevertheless, we have achieved the synthesis of a variety of supported intermetallic nanoparticles,<sup>4,6</sup> including those using three elements; for example, Pt<sub>3</sub>Fe<sub>1–x</sub>M<sub>x</sub> (M = Co, Ni, Cu, Zn, Ga, In, Sn, Pb)<sup>20</sup> and PtGa with deposition of Pb, In, or Sn.<sup>21</sup>

In what follows, we report the synthesis of SiO<sub>2</sub> supported Co<sub>2</sub>FeGe nanoparticles and its catalytic properties for selective

<sup>a</sup>Frontier Research Institute for Interdisciplinary Sciences, Tohoku University, Sendai, Japan

<sup>b</sup>Institute of Multidisciplinary Research for Advanced Materials, Tohoku University, Sendai, Japan

<sup>c</sup>Institute for Catalysis, Hokkaido University, Sapporo, Japan. E-mail: furukawa@cat.hokudai.ac.jp

† Electronic supplementary information (ESI) available. See DOI: 10.1039/d1ra02884g

‡ T. K. and S. F. equally contributed to this work.

§ Present address: Division of Chemistry and Materials, Faculty of Textile Science and Technology, Shinshu University, Japan. E-mail: tkojima@shinshu-u.ac.jp



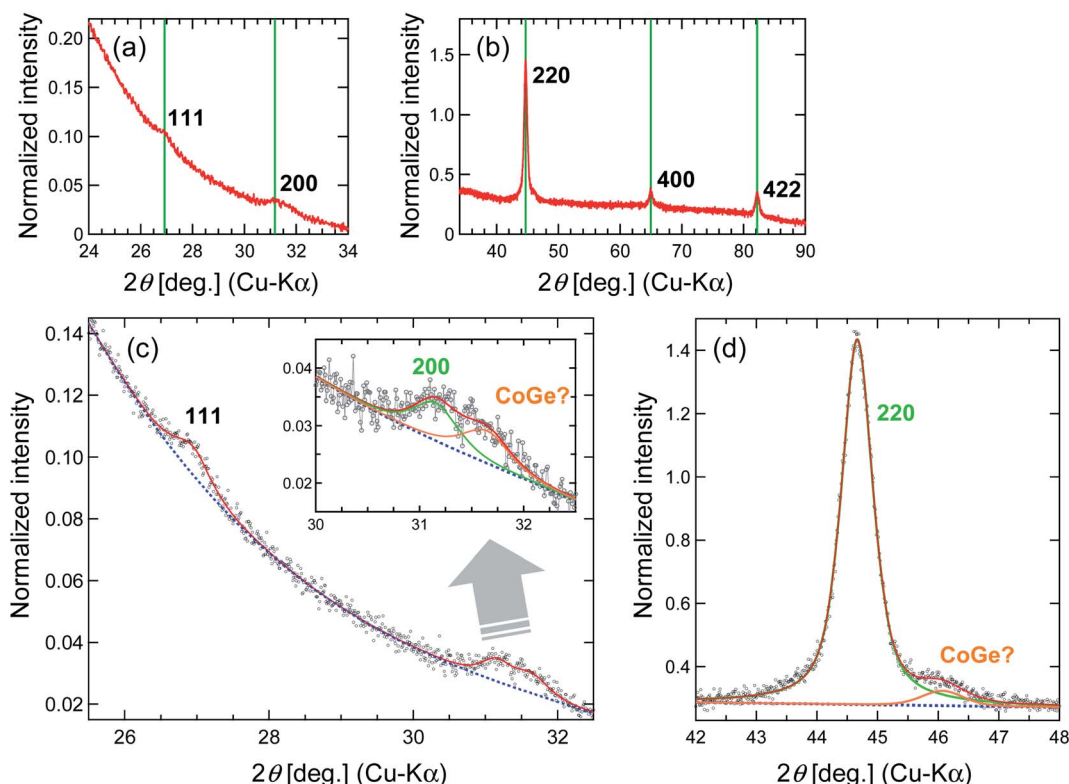
hydrogenation of propyne ( $C_3H_4$ ). The Co-based catalysts were prepared by the pore-filling (co-)impregnation method using  $SiO_2$  as the support.  $Co(NO_3)_3 \cdot 6H_2O$  (Wako, 98%),  $Fe(NO_3)_3 \cdot 9H_2O$  (Sigma-Aldrich, 98%),  $(NH_4)_2GeF_6$  (Aldrich, 99.9%) were used as the metal precursors, and the Co loading was adjusted at 3 wt%. The metal precursors were precisely weighed and dissolved together in deionized water so that the Co : Fe : Ge atomic ratio was 1.8 : 1 : 1. A mixed aqueous solution of metal precursors was added dropwise to ground dried silica gel (CARIACT G-6, Fuji Silysia,  $S_{BET} = 673 \text{ m}^2 \text{ g}^{-1}$ ) so that the solutions just filled the pores of the silica gel (volume of solution: 1.6 mL per gram of silica). The mixtures were sealed with a piece of plastic film and kept overnight at room temperature, followed by freeze-drying under vacuum at 0 °C and further drying overnight in an oven at 90 °C. The resulting powder was calcined in air at 500 °C for 1 h, then reduced under flowing  $H_2$  (0.1 MPa, 50 mL  $\text{min}^{-1}$ ) at 800 °C for 1 h.

Fig. 1 shows the powder X-ray diffraction (XRD) (Rigaku Ultima IV) pattern for the synthesized  $Co_2FeGe/SiO_2$ . Although tiny peaks of another phase (possibly CoGe) were detected by peak fitting, as shown in Fig. 1c and d, all visible peaks in Fig. 1a and b are assigned to  $Co_2FeGe$  Heusler phase ( $L2_1$  structure). The peaks were broad, indicating the formation of nano-sized grains. The volume-weighted average grain size ( $d_{XRD}$ ) was

roughly estimated to be 13 nm from the full width at half maximum (FWHM) of the 220 peak using the Scherrer equation:

$$d_{XRD} = K\lambda/W \cos \theta \quad (1)$$

where  $K$ ,  $\lambda$ , and  $W$  are the Scherrer constant, a wavelength, and a peak width, respectively; and  $8/3\pi$  and FWHM were respectively adopted as  $K$  and  $W$  based on the assumption of spherical crystallites with lognormal size distribution.<sup>22</sup> 111 and 200 superlattice peaks were certainly observed, meaning the formation of the ordered structure. These peaks are essentially very weak, because their intensities ( $I$ ) are proportional to the square of the difference in the atomic scattering factors ( $F$ ) of constituents, which are basically proportional to atomic numbers ( $I_{111} \propto |F_{Fe} - F_{Ge}|^2$ ,  $I_{200} \propto |F_{Co} - (F_{Fe} + F_{Ge})/2|^2$ ). Considering the anomalous scattering factors,<sup>23</sup> the Debye-Waller factors,<sup>24,25</sup> the multiplicity factor, and the Lorentz-polarization factor,  $I_{111}/I_{220} = 0.007$  and  $I_{200}/I_{220} = 0.004$  are derived for the perfectly ordered case. The broadening also makes it difficult to detect the superlattice peaks. Thus, the detection of the superlattice peaks indicates that the  $L2_1$ -ordered structure correctly formed even in nanograins. The degree of long-range order for Heusler alloys is evaluated typically by Webster's model using  $S$  and  $\alpha$ <sup>10,26,27</sup> as



**Fig. 1** XRD patterns for  $Co_2FeGe/SiO_2$  (a) around superlattice peaks, (b) around fundamental peaks, (c) around superlattice peaks with fitting, and (d) around 220 peak with fitting. All peaks were normalized by integrated intensity of 220 peak. Green vertical lines in (a) and (b) show peak positions observed for unsupported  $Co_2FeGe$  powders. Blue dashed lines and red solid lines in (c) and (d) show backgrounds and sum of fitting lines, respectively. Inset of (c) displays magnification around 200 peak with fitting lines for 200 peak (green) and for second phase peak (orange) possibly originating from intermetallic CoGe phase, which also has a peak (orange) nearby 220 peak (green) in (d). Fitting was done using pseudo-Voigt function for peaks and polynomial function for backgrounds.

$$S = \sqrt{\frac{(I_{200}/I_{400})_{\text{exp}}}{(I_{200}/I_{400})_{\text{cal}}}} \quad (2)$$

$$(1 - 2\alpha)S = \sqrt{\frac{(I_{111}/I_{\text{fund}})_{\text{exp}}}{(I_{111}/I_{\text{fund}})_{\text{cal}}}} \quad (3)$$

where  $I_{200}$ ,  $I_{111}$ , and  $I_{\text{fund}}$  are integrated intensities of 200 and 111 superlattice peaks, and a fundamental peak, respectively, and “exp” and “cal” respectively, means an experimental value and a calculated one for the perfectly ordered case.  $S$  corresponds to the long-range order parameter for binary alloys,<sup>28</sup> here describing the order between Co and Fe or Ge atoms ( $0 \leq S \leq 1$ );  $\alpha$  describes the disorder between Fe and Ge atoms ( $0 \leq \alpha \leq 0.5$ ); thus,  $S = 1$  with  $\alpha = 0$  means the perfect order. Although accurate evaluation of  $I_{200}$  and  $I_{111}$  was difficult because of too small an intensity,  $S$  and  $\alpha$  were roughly estimated to be 0.8 and 0.0, respectively, when using the fitted data in Fig. 1c. Thus, the degree of long-range order was likely high.

Fig. 2a shows the image obtained by high-resolution high-angle annular dark field scanning transmission electron microscopy (HAADF-STEM) (FEI Titan G2). Brighter particles with relatively uniform diameters below about 30 nm are observed on darker skeletal matter, which indicates that

$\text{Co}_2\text{FeGe}$  nanoparticles are relatively homogeneously distributed on  $\text{SiO}_2$  supports. The diameters of the brighter particles were counted, as shown in Fig. 2b. The size distribution was relatively narrow. The volume-weighted average diameter ( $d_{\text{TEM}}$ ) was estimated to be  $23.0 \pm 5.3$  nm by

$$d_{\text{TEM}} = \Sigma n_i d_i^4 / \Sigma n_i d_i^3 \quad (4)$$

where  $n_i$  is the number of particles with the diameter  $d_i$  in Fig. 2b.<sup>20,21</sup> Fig. 2c–f show elemental maps obtained by energy-dispersive X-ray (EDX) analysis. Co, Fe, and Ge were detected in the same regions, in which the brighter particles were observed in Fig. 2a. The quantitative analysis for the particle represented in Fig. 2g revealed that the chemical composition among Co, Fe, and Ge followed the precursor ratio and was close to the stoichiometry, as shown in Fig. 2h. These XRD and HAADF-STEM results clearly indicate the success of synthesizing  $\text{Co}_2\text{FeGe}$  nanoparticles on  $\text{SiO}_2$  supports of sufficient quality.

The  $\text{Co}_2\text{FeGe}/\text{SiO}_2$  was tested for catalytic reaction of the  $\text{C}_3\text{H}_4$  hydrogenation using a standard flow reactor (see ref. 11 for details). Thirty mg of the catalyst was heated under  $\text{H}_2$  gas flow at 800 °C for 1 h to remove surface oxides; then, feeding of a gaseous mixture of [0.1%  $\text{C}_3\text{H}_4$ /40%  $\text{H}_2$ /He balance] began at

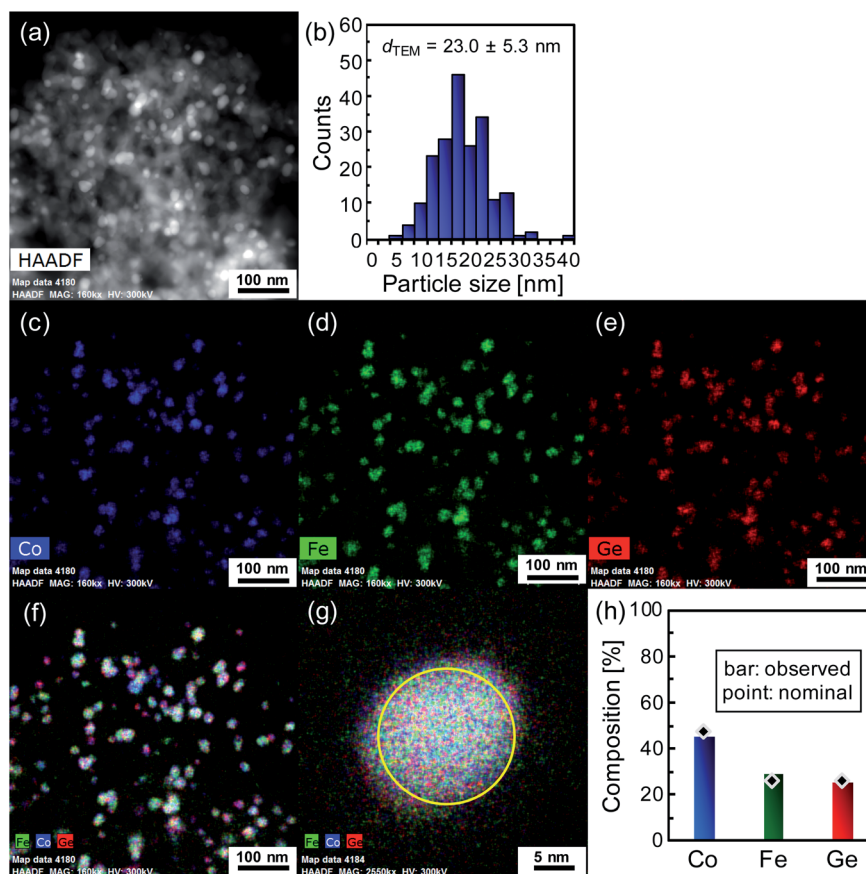


Fig. 2 Analysis by HAADF-STEM with EDX for  $\text{Co}_2\text{FeGe}/\text{SiO}_2$ : (a) HAADF-STEM image, (b) histogram of diameter for bright particles in (a), elemental maps for (c) Co, (d) Fe, and (e) Ge, (f) superimposed elemental map, (g) magnified elemental map, and (h) chemical composition in area marked by yellow circle in (g). In (h) bars display observed values and points indicate nominal values estimated from precursor ratio.



ambient temperature and pressure at 30 mL min<sup>-1</sup> (20 °C, 0.1 MPa) (space velocity: about 40 000 h<sup>-1</sup>). The products were analyzed by gas chromatography (Agilent 490 Micro GC with PoraPLOT Q column) after waiting 30 min at each temperature. The conversion of C<sub>3</sub>H<sub>4</sub> and the selectivity of products were estimated by

$$\text{Conversion} = 100 \times \frac{C_{\text{feed}} - C_{\text{unreact}}}{C_{\text{feed}}} [\%] \quad (5)$$

$$\text{Selectivity} = 100 \times \frac{C_{\text{C}_3\text{H}_6} \text{ or } C_{\text{C}_3\text{H}_8} \text{ or } C_{\text{lost}}}{C_{\text{C}_3\text{H}_6} + C_{\text{C}_3\text{H}_8} + C_{\text{lost}}} [\%] \quad (6)$$

where  $C_{\text{feed}}$ ,  $C_{\text{unreact}}$ ,  $C_{\text{C}_3\text{H}_6}$ , and  $C_{\text{C}_3\text{H}_8}$  were the concentrations of the feed C<sub>3</sub>H<sub>4</sub>, the unreacted C<sub>3</sub>H<sub>4</sub>, the produced C<sub>3</sub>H<sub>6</sub>, and the produced C<sub>3</sub>H<sub>8</sub>, respectively.  $C_{\text{lost}}$  is the concentration of carbon species lost due to oligomerization or coking, which is estimated by  $C_{\text{lost}} = C_{\text{feed}} - C_{\text{unreact}} - C_{\text{C}_3\text{H}_6} - C_{\text{C}_3\text{H}_8}$ .

Fig. 3a shows the results of the catalytic test. The carbon lost was negligible. The C<sub>3</sub>H<sub>6</sub> selectivity was as high as over 70% even when the C<sub>3</sub>H<sub>4</sub> conversion was 100%. In general, strong adsorption of C<sub>3</sub>H<sub>4</sub> prevents re-adsorption of C<sub>3</sub>H<sub>6</sub>, which suppresses the further hydrogenation of C<sub>3</sub>H<sub>6</sub>, resulting in high C<sub>3</sub>H<sub>6</sub> selectivity when the C<sub>3</sub>H<sub>4</sub> conversion is below 100%. Once all C<sub>3</sub>H<sub>4</sub> is consumed, C<sub>3</sub>H<sub>6</sub> is quickly hydrogenated; thus, the C<sub>3</sub>H<sub>6</sub> selectivity drastically decreases once the C<sub>3</sub>H<sub>4</sub> conversion achieves 100% in most catalysts, including pure metals<sup>29,30</sup> and Co<sub>2</sub>FeGe<sup>11</sup> (Fig. S1a and b†). Therefore, the Co<sub>2</sub>FeGe/SiO<sub>2</sub> synthesized here has an intrinsic selectivity for C<sub>3</sub>H<sub>6</sub> as well as the unsupported Co<sub>2</sub>FeGe powders synthesized metallurgically, the C<sub>3</sub>H<sub>6</sub> selectivity of which was over 90% even when the C<sub>3</sub>H<sub>4</sub> conversion was 100% (Fig. S2†).<sup>11</sup> The reaction rate per weight of Co used was significantly enhanced up to as much as 2000 times by nano-sizing compared with the unsupported one, as shown in Fig. 3b. In terms of stability, a small deactivation was observed in the cooling process after heating up to 200 °C (Fig. S3†), likely due to oligomerization or coking, while the C<sub>3</sub>H<sub>6</sub> selectivity was improved over 90%.

To reveal the reason for the lower C<sub>3</sub>H<sub>6</sub> selectivity of the Co<sub>2</sub>FeGe/SiO<sub>2</sub> than that of the unsupported Co<sub>2</sub>FeGe, the catalytic test for C<sub>3</sub>H<sub>6</sub> hydrogenation was conducted in the same manner as the C<sub>3</sub>H<sub>4</sub> hydrogenation as shown in Fig. 3c. A certain amount of C<sub>3</sub>H<sub>6</sub> was converted to C<sub>3</sub>H<sub>8</sub>, whereas it was

scarcely converted by the unsupported one.<sup>11</sup> This means the presence of the sites that further hydrogenate C<sub>3</sub>H<sub>6</sub> in the C<sub>3</sub>H<sub>4</sub> hydrogenation. For ordinary catalysts, the conversion is larger for the C<sub>3</sub>H<sub>6</sub> hydrogenation than C<sub>3</sub>H<sub>4</sub> hydrogenation at a lower temperature region in these reaction conditions<sup>11</sup> (Fig. S1†). The larger conversion of C<sub>3</sub>H<sub>6</sub> than C<sub>3</sub>H<sub>4</sub> at ≤75 °C for the Co<sub>2</sub>FeGe/SiO<sub>2</sub> (Fig. 3a and c) thus also indicates the presence of non-selective sites for the C<sub>3</sub>H<sub>4</sub> hydrogenation. An anomaly at 175 °C in Fig. 3c is likely a result of conflict between the acceleration of reaction and the deceleration of C<sub>3</sub>H<sub>6</sub> adsorption along with increasing temperature, which is often observed.<sup>11</sup>

Taking into account the origin of the high alkene selectivity that inactive Ge atoms shrink the size of active ensembles and thereby prevent the re-adsorption of alkene molecules, which is indicated from electronic structures,<sup>11</sup> two candidates are considered for the non-selective sites. One is a monometallic Co ensemble. In this impregnation synthesis, a part of the particles likely have chemical compositions that deviate from the target value. In particles with excess Co, monometallic Co ensembles should form, which is active for hydrogenation but not selective, as indicated by the tests using Co/SiO<sub>2</sub> (Fig. S1a and c†). Actually, Co<sub>2</sub>FeGe/SiO<sub>2</sub> catalysts preliminary prepared with the atomic ratio of Co : Fe : Ge = 2 : 1 : 1 loaded exhibited a poor selectivity (Fig. S4a†) in contrast to the present catalyst (loaded Co : Fe : Ge = 1.8 : 1 : 1), and the former showed an extra peak in the temperature programmed CO desorption profile as well as the pure Co in addition to the peaks for the unsupported Co<sub>2</sub>FeGe (Fig. S4b†).<sup>31</sup> The other candidate for non-selective sites is a specific site formed by nano-sizing, such as the corner and the edge. These low-coordinated sites are generally active but in different environments from the terrace sites; thus, they can be non-selective. A tiny amount of the second phase CoGe is unlikely as the candidate because a high ethylene selectivity in selective hydrogenation of acetylene by CoGe has been reported.<sup>32</sup>

Although it cannot be concluded whether the Co ensembles or the specific sites dominated the reduction of selectivity, the selectivity will increase up to the value for the unsupported one if the non-selective sites are identified and removed. Actually, the C<sub>3</sub>H<sub>6</sub> selectivity was improved along with the deactivation

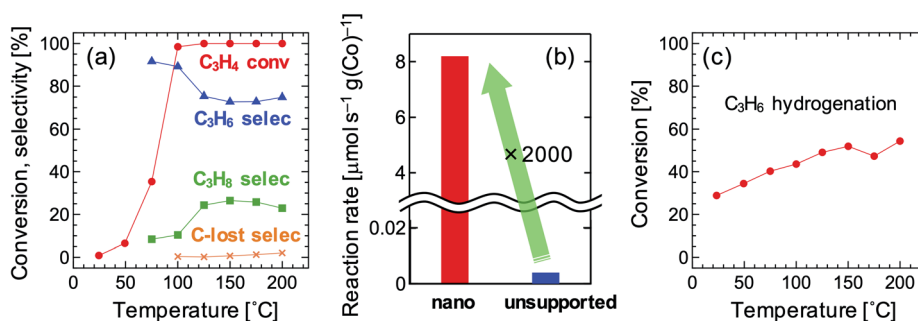


Fig. 3 (a) Catalytic properties of Co<sub>2</sub>FeGe/SiO<sub>2</sub> for C<sub>3</sub>H<sub>4</sub> hydrogenation, (b) C<sub>3</sub>H<sub>4</sub> reaction rate per weight of Co at 75 °C for Co<sub>2</sub>FeGe/SiO<sub>2</sub> ("nano") and unsupported Co<sub>2</sub>FeGe ("unsupported"), (c) C<sub>3</sub>H<sub>6</sub> conversion for Co<sub>2</sub>FeGe/SiO<sub>2</sub> in C<sub>3</sub>H<sub>6</sub> hydrogenation. Reaction conditions in (c) were the same as those in (a) except the reactant, which was [0.1% C<sub>3</sub>H<sub>6</sub>/40% H<sub>2</sub>/He-balance] in (c).





Table 1 Catalytic performance of supported intermetallic catalysts for selective hydrogenation of alkynes. C<sub>2</sub>H<sub>2</sub>/C<sub>2</sub>H<sub>4</sub> was used as a reactant in literature

Catalyst	Ni(Co) wt %	Amount [mg]	C <sub>2</sub> H <sub>2</sub> (C <sub>3</sub> H <sub>4</sub> ) flow rate [mL min <sup>-1</sup> ]	C <sub>2</sub> H <sub>2</sub> (C <sub>3</sub> H <sub>4</sub> ) : H <sub>2</sub> : C <sub>2</sub> H <sub>4</sub> (C <sub>3</sub> H <sub>6</sub> ) : He(Ar, N <sub>2</sub> )	GHSV [mL g <sup>-1</sup> h <sup>-1</sup> ]	Conv. [%]	Selec. [%]	Temp. [°C]	Specific rate [mL C <sub>3</sub> H <sub>6</sub> (C <sub>3</sub> H <sub>4</sub> ) min <sup>-1</sup> g <sub>Ni(Co)</sub> <sup>-1</sup> ]	Ref.
Ni <sub>3</sub> Ge/MCM-41	3.2	16	3.9	3.9 : 8 : 0 : 17.1	107520	30	85	250	2340	33
NiGa/Mg/Al-LDH	10	50	1.2	1.2 : 12 : 0 : 106.8	144000	94	81	220	226	34
			1.2	1.2 : 12 : 24 : 82.8	144000	72	82	100	62	
						7	75	186	173	
Ni <sub>3</sub> Ga/MgAl <sub>2</sub> O <sub>4</sub>	2	100	0.33	0.33 : 6.7 : 33.3 : 26.67	40 000	91	87	93	17	35
						9	77	200	152	
Co <sub>2</sub> FeGe/SiO <sub>2</sub>	3	30	0.03	0.03 : 12 : 0.17.97	60 000	98	96	100	15	This work
	3	60	0.03	0.03 : 12 : 3 : 14.97	30 000	98	89	100	33	
							77	100	16	

(Fig. S3†), indicating that the non-selective sites were killed by carbon deposition due to oligomerization or coking. Nevertheless, over 70% for C<sub>3</sub>H<sub>6</sub> selectivity at 100% conversion of C<sub>3</sub>H<sub>4</sub> is high enough for the condition under abundant hydrogen (C<sub>3</sub>H<sub>4</sub> : H<sub>2</sub> = 1 : 400). This high selectivity was also confirmed in the C<sub>3</sub>H<sub>4</sub> hydrogenation in the presence of abundant C<sub>3</sub>H<sub>6</sub> (Fig. S5†). These results indicate that the excellent catalytic properties of intermetallic micro-powders can be conserved in their nanoparticles. The reaction rate of C<sub>3</sub>H<sub>4</sub> per surface area of Co<sub>2</sub>FeGe was roughly estimated to be  $1.2 \times 10^{-7} \text{ mol s}^{-1} \text{ m}^{-2}$  at 75 °C by assuming the 23 nm-spheres with density of  $8.66 \text{ g cm}^{-3}$  (estimated by XRD for the unsupported one and using atomic weights). The value for the unsupported one was  $4.1 \times 10^{-8} \text{ mol s}^{-1} \text{ m}^{-2}$  at 75 °C. Although the estimation was very approximate, it can at least be said that the reaction rate did not decrease, or rather, it seems that the reaction rate somewhat increased by nano-sizing. This fact also assures the conservation of intrinsic catalytic properties after nano-sizing, while which increases the surface energy, enhancing the adsorption of reactant species, thereby possibly increasing the reaction rate.

The catalytic performance is compared with those of other supported intermetallic catalysts reported (Table 1). Since Ni is a typical catalyst for hydrogenation, 3d-transition-metal-based intermetallic catalysts reported for selective hydrogenation of alkynes are mostly Ni-based. Although the performance cannot be exactly compared, because the reported catalysts were tested for selective hydrogenation of acetylene (C<sub>2</sub>H<sub>2</sub>) with different reaction conditions, the selectivity of Co<sub>2</sub>FeGe/SiO<sub>2</sub> seems to be at the same level as those of the reported catalysts. By comparing a specific reaction rate per weight of Ni or Co at 100 °C, the activity of Co<sub>2</sub>FeGe/SiO<sub>2</sub> also seems to be at the same level as those of the reported catalysts.

## Conclusions

We have successfully synthesized the SiO<sub>2</sub> supported Co<sub>2</sub>FeGe nanoparticles by the co-impregnation method. The XRD indicated that the sample was almost a single phase of a highly ordered Heusler structure. The HAADF-STEM with EDX indicated that Co<sub>2</sub>FeGe nanoparticles with the average size of 23 nm were relatively homogeneously distributed on SiO<sub>2</sub> supports. This nano-sizing enhanced the reaction rate per weight for C<sub>3</sub>H<sub>4</sub> hydrogenation by 2000 times compared with the unsupported powders, while conserving high C<sub>3</sub>H<sub>6</sub> selectivity. This study proves that even ternary intermetallic compounds can be downsized into supported nanoparticles with conserving intrinsic catalytic properties. In future, supported nanoparticles of various ternary intermetallic compounds including Heusler alloys would be developed not only as catalysts but also as other functional materials.

## Conflicts of interest

There are no conflicts to declare.



## Acknowledgements

We are grateful to the technical staffs of faculty of engineering, Hokkaido University for HAADF-STEM/EDX analysis. This work was conducted under the Cooperative Research Program of Institute for Catalysis, Hokkaido University (Grant #20B1006 and #21A1004). A part of this work was supported by JSPS KAKENHI grant number JP19H02452, 17H04965, and 20H02517, and the Sumitomo Electric Industries Group CSR Foundation.

## References

- 1 A. P. Tsai, S. Kameoka and Y. Ishii, *J. Phys. Soc. Jpn.*, 2004, **73**, 3270–3273.
- 2 M. Armbrüster, R. Schlögl and Y. Grin, *Sci. Technol. Adv. Mater.*, 2014, **15**, 034803.
- 3 A. P. Tsai, S. Kameoka, K. Nozawa, M. Shimoda and Y. Ishii, *Acc. Chem. Res.*, 2017, **50**, 2879–2885.
- 4 S. Furukawa and T. Komatsu, *ACS Catal.*, 2017, **7**, 735–765.
- 5 M. Armbrüster, *Sci. Technol. Adv. Mater.*, 2020, **21**, 303–322.
- 6 S. Furukawa, T. Komatsu and K. Shimizu, *J. Mater. Chem. A*, 2020, **8**, 15620–15645.
- 7 J. Dshemuchadse and W. Steurer, *Acta Crystallogr.*, 2015, **A71**, 335–345.
- 8 Y. Gong, J. Wu, M. Kitano, J. Wang, T. N. Ye, J. Li, Y. Kobayashi, K. Kishida, H. Abe, Y. Niwa, H. Yang, T. Tada and H. Hosono, *Nat. Catal.*, 2018, **1**, 178–185.
- 9 J. Wu, J. Li, Y. Gong, M. Kitano, T. Inoshita and H. Hosono, *Angew. Chem., Int. Ed.*, 2019, **58**, 825–829.
- 10 T. Kojima, S. Kameoka and A.-P. Tsai, *ACS Omega*, 2017, **2**, 147–153.
- 11 T. Kojima, S. Kameoka, S. Fujii, S. Ueda and A.-P. Tsai, *Sci. Adv.*, 2018, **4**, eaat6063.
- 12 T. Kojima, S. Kameoka and A.-P. Tsai, *Sci. Technol. Adv. Mater.*, 2019, **20**, 445–455.
- 13 T. Kojima, S. Kameoka and A.-P. Tsai, *ACS Omega*, 2019, **4**, 21666–21674.
- 14 T. Kojima, S. Kameoka and A.-P. Tsai, *KONA Powder Part. J.*, 2021, **38**, 110–121.
- 15 L. Basit, C. Wang, C. A. Jenkins, B. Balke, V. Ksenofontov, G. H. Fecher, C. Felser, E. Mugnaioli, U. Kolb, S. A. Nepijko, G. Schönhense and M. Klimenkov, *J. Phys. D: Appl. Phys.*, 2009, **42**, 084018.
- 16 C. Wang, L. Basit, Y. Khalavka, Y. Guo, F. Casper, T. Gasi, V. Ksenofontov, B. Balke, G. H. Fecher, C. Sönnichsen, Y. K. Hwu, J. J. Lee and C. Felser, *Chem. Mater.*, 2010, **22**, 6575–6582.
- 17 C. H. Wang, Y. Z. Guo, F. Casper, B. Balke, G. H. Fecher, C. Felser and Y. Hwu, *Appl. Phys. Lett.*, 2010, **97**, 103106.
- 18 C. Wang, F. Casper, Y. Guo, T. Gasi, V. Ksenofontov, B. Balke, G. H. Fecher, C. Felser, Y. K. Hwu and J. J. Lee, *J. Appl. Phys.*, 2012, **112**, 124314.
- 19 S. Ernst, O. Malter, A. Schuessler, K. Braunsman, N. Trukhan and U. Mueller, inventor; BASF, SE, assignee, *US Pat.*, US 2019/0358613 A1, 2019.
- 20 Y. Nakaya, M. Miyazaki, S. Yamazoe, K. Shimizu and S. Furukawa, *ACS Catal.*, 2020, **10**, 5163–5172.
- 21 Y. Nakaya, J. Hirayama, S. Yamazoe, K. Shimizu and S. Furukawa, *Nat. Commun.*, 2020, **11**, 2838.
- 22 T. Ida, S. Shimazaki, H. Hibino and H. Toraya, *J. Appl. Crystallogr.*, 2003, **36**, 1107–1115.
- 23 S. Sasaki, *KEK Report*, 1989, **88–14**, pp. 1–136, calculated values can be downloaded from <http://www.sasakiken.net/indexe.html>.
- 24 N. M. Butt and J. Bashir, *Acta Crystallogr., Sect. A: Found. Crystallogr.*, 1988, **44**, 396–398.
- 25 *International Tables for Crystallography Vol C Mathematical, Physical and Chemical Tables*, ed. E. Prince, Kluwer Academic Publishers, 3rd edn, London, 2004, p. 239.
- 26 T. Kojima, S. Kameoka and A.-P. Tsai, *ACS Omega*, 2018, **3**, 9738.
- 27 P. J. Webster and K. R. A. Ziebeck, *J. Phys. Chem. Solids*, 1973, **34**, 1647–1654.
- 28 B. E. Warren, *X-Ray Diffraction*, Dover Publications, New York, 1990, p. 208.
- 29 N. Yoshida, PhD thesis, Osaka University, Japan, 1971.
- 30 T. Kojima, S. Fujieda, G. Kato, S. Kameoka, S. Suzuki and A. P. Tsai, *Mater. Trans.*, 2017, **58**, 776–781.
- 31 T. Kojima, T. Koganezaki, S. Fujii, S. Kameoka and A.-P. Tsai, *Catal. Sci. Technol.*, 2021, DOI: 10.1039/D1CY00279A.
- 32 T. Komatsu, M. Fukui and T. Yashima, *Stud. Surf. Sci. Catal.*, 1996, **101**, 1095–1104.
- 33 T. Komatsu, T. Kishi and T. Gorai, *J. Catal.*, 2008, **259**, 174–182.
- 34 Y. Cao, H. Zhang, S. Ji, Z. Sui, Z. Jiang, D. Wang, F. Zaera, X. Zhou, X. Duan and Y. Li, *Angew. Chem., Int. Ed.*, 2020, **59**, 11647–11652.
- 35 Y. Liu, X. Liu, Q. Feng, D. He, L. Zhang, C. Lian, R. Shen, G. Zhao, Y. Ji, D. Wang, G. Zhou and Y. Li, *Adv. Mater.*, 2016, **28**, 4747–4754.

